THE JOURNAL OF BIOLOGICAL CHEMISTRY VOL. 281, NO. 46, pp. 34897–34908, November 17, 2006
Printed in the U.S.A.

The Chemistry of Phospholipid Binding by the *Saccharomyces cerevisiae* Phosphatidylinositol Transfer Protein Sec14p as Determined by EPR Spectroscopy*

Received for publication, March 30, 2006, and in revised form, August 31, 2006 Published, JBC Papers in Press, September 22, 2006, DOI 10.1074/jbc.M603054200

Tatyana I. Smirnova[‡1], Thomas G. Chadwick[‡], Ryan MacArthur[‡], Oleg Poluektov[§], Likai Song[¶], Margaret M. Ryan[‖2], Gabriel Schaaf[‖2,3], and Vytas A. Bankaitis[‖4]

From the [‡]Department of Chemistry, North Carolina State University, Raleigh, North Carolina 27695, [§]Argonne National Laboratory, Argonne, Illinois 60439, [¶]Florida State University, Tallahassee, Florida 32310, and the [‖]Department of Cell and Developmental Biology, Lineberger Comprehensive Cancer Center, University of North Carolina, Chapel Hill, North Carolina 27599-7090

The major yeast phosphatidylinositol/phosphatidylcholine transfer protein Sec14p is the founding member of a large eukaryotic protein superfamily. Functional analyses indicate Sec14p integrates phospholipid metabolism with the membrane trafficking activity of yeast Golgi membranes. In this regard, the ability of Sec14p to rapidly exchange bound phospholipid with phospholipid monomers that reside in stable membrane bilayers is considered to be important for Sec14p function in cells. How Sec14p-like proteins bind phospholipids remains unclear. Herein, we describe the application of EPR spectroscopy to probe the local dynamics and the electrostatic microenvironment of phosphatidylcholine (PtdCho) bound by Sec14p in a soluble protein-PtdCho complex. We demonstrate that PtdCho movement within the Sec14p binding pocket is both anisotropic and highly restricted and that the C_5 region of the *sn*-2 acyl chain of bound PtdCho is highly shielded from solvent, whereas the distal region of that same acyl chain is more accessible. Finally, high field EPR reports on a heterogeneous polarity profile experienced by a phospholipid bound to Sec14p. Taken together, the data suggest a headgroup-out orientation of Sec14p-bound PtdCho. The data further suggest that the Sec14p phospholipid binding pocket provides a polarity gradient that we propose is a primary thermodynamic factor that powers the ability of Sec14p to abstract a phospholipid from a membrane bilayer.

Phosphatidylinositol transfer proteins (PITPs)[5] represent a subset of a larger group of phospholipid transfer proteins that are operationally defined by their ability to mobilize phospholipids between membrane bilayers *in vitro*. PITPs catalyze such energy-independent transfer of either phosphatidylinositol (PtdIns) or phosphatidylcholine (PtdCho) between membrane bilayers *in vitro*, with PtdIns representing the preferred ligand in the transfer reactions (1, 2). PITPs themselves are highly conserved across the eukaryotic kingdom and fall into two distinct classes based upon primary sequence and structural fold (reviewed in Ref. 2). These two classes are defined as the Sec14p-like PITPs and the unrelated metazoan PITPs. Deficiencies in metazoan PITP functions are either cell-lethal in mammals or, in the case of PITP-α isoform, result in neurodegenerative, glucose homeostatic, and intestinal malabsorbtion diseases in mice (3). Sec14p domain proteins are also of medical interest, since inherited disorders, such as vitamin E-responsive ataxia, ataxia/dystonia in the *jittery* mouse, etc., are associated with individual defects in them (4, 5). Moreover, the developmental switch from yeast to mycelial growth modes, a morphogenetic program whose execution is essential for the pathogenesis of dimorphic yeast, is also regulated by Sec14p isoforms (6, 7). The preponderance of evidence indicates that PITPs integrate the action of specific phospholipid metabolic reactions with regulation of specific membrane trafficking processes.

The largest and most widely distributed PITP class is represented by the Sec14p-like proteins, so named on the basis of the founding member of the family, the yeast Sec14p PITP. The Sec14p-like PITP class consists of nearly 300 members, and it is appropriate to consider this large group of proteins as the Sec14p superfamily (2). The Sec14p lipid binding domain is employed in a binding strategy for a diverse set of hydrophobic ligands (*e.g.* phospholipids, phosphoinositides, sterol precursors, retinal, and tocopherols) and can be expressed either as a free standing domain or as one that is integrated into multidomain modules. The simple budding yeast *S. cerevisiae* expresses six Sec14ps, and this protein class is more highly expanded in higher eukaryotes (*e.g.* at least 31 members in *Arabidopsis*) (8).

* The work at North Carolina State University was supported by National Science Foundation Grant MCB-0451510 with partial support from American Chemical Society Petroleum Research Fund Grant 40771-G4 (both to T. I. S.). The work at Argonne National Laboratory was supported by the United States Department of Energy, Office of Basic Energy Sciences, Division of Chemical Sciences, Geosciences, and Biosciences, under Contract W-31-109-Eng-38. The National Biomedical EPR Center is supported by National Institutes of Health (NIH) Grant EB001980. The costs of publication of this article were defrayed in part by the payment of page charges. This article must therefore be hereby marked "*advertisement*" in accordance with 18 U.S.C. Section 1734 solely to indicate this fact.

[1] To whom correspondence may be addressed: Dept. of Chemistry, North Carolina State University, 2620 Yarborough Dr., Raleigh, NC 27695. Tel.: 919-513-4375; Fax: 919-513-7353; E-mail: Tatyana_Smirnova@ncsu.edu.

[2] Supported by NIH Grant GM44530 (to V. A. B.).
[3] Supported by a postdoctoral training grant from the Deutsche Forschungsgemeinschaft.

[4] To whom correspondence may be addressed: Dept. of Cell & Developmental Biology, 108 Taylor Hall, University of North Carolina, Chapel Hill, NC 27599-7090. Tel.: 919-962-9870; Fax: 919-966-1856; E-mail: vytas@med.unc.edu.

[5] The abbreviations used are: PITP, phosphatidylinositol transfer protein; PtdIns, 1,2-dioleoyl-*sn*-glycero-3-phosphoinositol (ammonium salt); 10-doxyl-PtdCho, 1-acyl-2-(10-(doxyl)stearoyl)-*sn*-glycero-3-phosphocholine; 16-doxyl-PtdCho, 1-acyl-2-(16-(doxyl)stearoyl)-sn-glycero-3-phosphocholine.

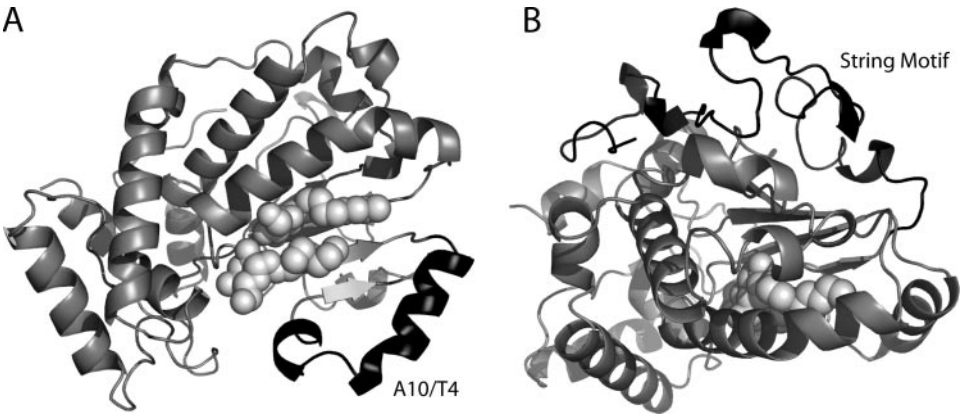

FIGURE 1. **Crystal structure of the *S. cerevisiae* Sec14p.** The Sec14p fold (Protein Data Bank code 1AUA) (9) consists of 12 α-helices, six β-strands, and eight 3_{10}-helices. An *en face* view of the molecule that reveals the hydrophobic phospholipid binding pocket is shown in *ribbon diagram* mode (*A*). The Sec14p crystal structure is of an apo-form bound to two molecules of β-octyl glucoside (shown in space fill mode). These two detergent molecules reside in the single large hydrophobic pocket of the protein, and the pocket is proposed to be gated by the A10/T4 helix (in *black*; helix labeled), which is posited to reside in an "open" conformation in the apo-Sec14p structure. *B* depicts a view of the Sec14p molecule from the *top* so that the dominant structural element of the back of the molecule (the string motif; labeled and in *black*) is revealed. The string motif stabilizes the Sec14p fold by wrapping behind the β-strand floor of the hydrophobic pocket.

The available Sec14p crystal structure for Sec14p identifies a novel fold that forms a hydrophobic pocket of sufficient volume to accommodate a single molecule of PtdIns or PtdCho (Fig. 1) (9). The crystallizing unit is an apo-Sec14p loaded with two molecules of the detergent β-octyl glucoside. This particular structure is interpreted to describe a transitional Sec14p conformer that exists only transiently on the membrane surface as Sec14p undergoes phospholipid exchange. Although an understanding of how Sec14p functions at the molecular level is incomplete, the structural model spawned several hypotheses regarding intramolecular dynamic aspects of Sec14p function (9). First, an unusual surface helix (A10/T4) is identified as an attractive candidate for the structural element that "gates" the hydrophobic pocket (Fig. 1*A*). Second, a string motif that contains a series of four tightly wound 3_{10} helices wraps up the Sec14p fold and is suggested to play an important role in regulating conformational changes that accompany the phospholipid exchange reaction (Fig. 1*B*).

How Sec14p actually binds its phospholipid substrates remains an important and unanswered question. The available model provides considerable insight into how Sec14p might bind target membranes and individual phospholipids. With regard to substrate binding in the soluble Sec14p-phospholipid complex, bound phospholipid is predicted to orient with the acyl-chains packed into the hydrophobic interior of the pocket, whereas the phospholipid headgroup is disposed toward solvent. Although this hypothetical "headgroup-out" disposition of the bound phospholipid is both an attractive and an intuitive one, solution of a phospholipid-bound Sec14p structure is required to resolve this question, and no such information is yet available. Resolution of this issue is important, since it speaks to one of several potential mechanisms for how Sec14p (and Sec14p-like proteins) may regulate phospholipid metabolism. The uncertainty surrounding whether the intuitive orientation of phospholipid within the Sec14p pocket is indeed the correct one is emphasized by structural analyses of phospholipid-bound metazoan PITPs. These proteins bind phospholipid substrates in the reverse "headgroup-in" orientation (10, 11).

In this report, we describe our application of EPR spectroscopy to probe the local dynamics and the electrostatic microenvironment of a series of spin-labeled *n*-doxyl-PtdCho molecules incorporated into the Sec14p phospholipid binding pocket. We demonstrate that motion of PtdCho within the Sec14p binding pocket, while anisotropic and highly restricted, nonetheless exhibits a progressive increase in the mobility of the *sn*-2 acyl chain as distance from the headgroup/backbone region increases. Moreover, we show that the C_5 region of the *sn*-2 acyl chain is highly shielded from solvent, whereas the distal region of the acyl chain is less so. Finally, we describe evidence for a polar protic microenvironment at position C_5 of the *sn*-2 acyl chain that becomes increasingly aprotic as one moves away from the headgroup/backbone region of the bound phospholipid and returns to a more polar/protic environment at the distal end of the chain. These collective data are most consistent with a headgroup-out orientation of Sec14p-bound PtdCho and further indicate that the Sec14p phospholipid binding pocket provides a hydrophobic matching to accommodate the PtdCho molecule. We propose this polarity gradient is a primary thermodynamic factor that drives the ability of Sec14p to abstract a phospholipid from a membrane bilayer.

EXPERIMENTAL PROCEDURES

Expression and Purification of Sec14p—Recombinant His_6-Sec14p was purified from *Escherichia coli* essentially as previously described (9). Briefly, Sec14p expression in *E. coli* strain KK2186 (Δ*(lac-pro) supE thi strA sbcB-15 endA*/F′(*traD36 lacI*^{Q} *lacZ*Δ*15*)) was driven by a derivative of the pQE31 plasmid (Qiagen, Hilden, Germany) and induced with isopropyl β-thiogalactoside (1 mM final concentration). Bacterial cultures were incubated for an additional 5 h with shaking at 37 °C. Cells were harvested by centrifugation, and the cell pellet was resuspended in ice-cold lysis buffer (50 mM sodium phosphate, pH 7.1, 300 mM NaCl, 1 mM NaN_3, 0.2 mM phenylmethylsulfonyl fluoride). Lysozyme was added, and the suspension was incubated at 25 °C for an additional 10 min. Cells were disrupted by collision with 0.1-mm diameter glass beads in a cooled bead beater (Biospec Products, Bartlesville, OK). Cell lysates were subsequently clarified by differential centrifugation series at 1000 × *g*, 14,000 × *g*, and 100,000 × *g*, respectively. The clarified supernatant was applied to Talon™ Sepharose resin (Clontech), the resin was washed extensively with lysis buffer, and bound protein was eluted with a linear imidazole gradient (0–200 mM) reconstituted in lysis buffer. Peak fractions were

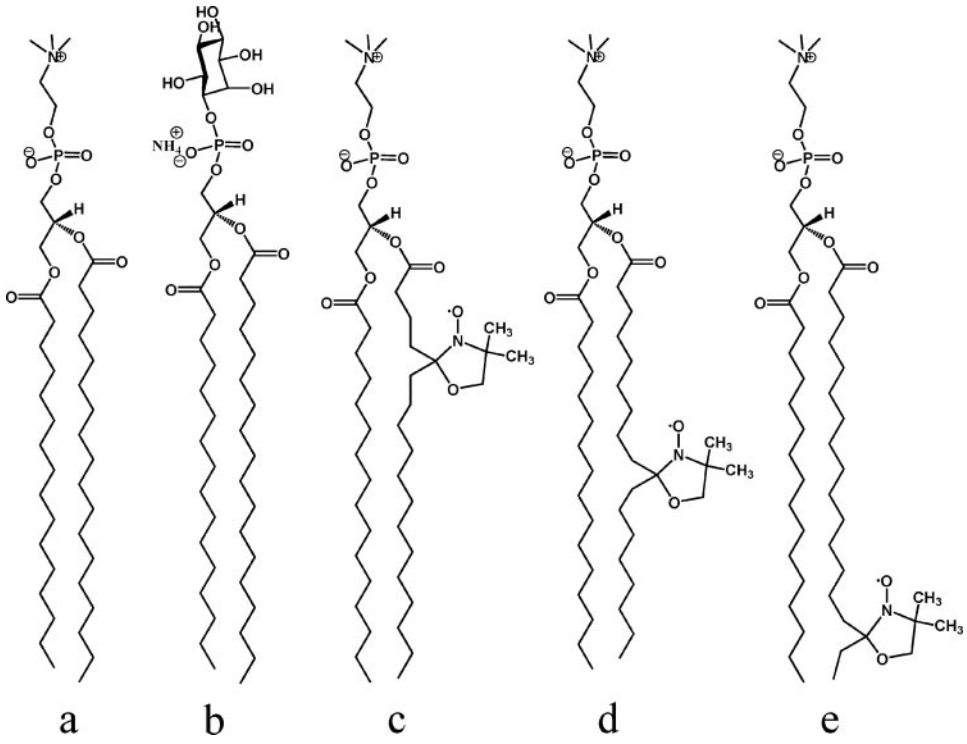

FIGURE 2. **Structure of lipids and selected spin probes used in this work: PtdCho (*a*), PtdIns (*b*), 5-doxyl-PtdCho (*c*), 10-doxyl-PtdCho (*d*), 16-doxyl-PtdCho (*e*).**

pooled and dialyzed extensively against lysis buffer at 4 °C, and a second round of affinity purification and dialysis was subsequently performed. Protein purity was monitored by SDS-PAGE and Coomassie Blue staining of gels. Sec14p purity exceeded 95%, and purified protein exhibited robust PtdIns and PtdCho transfer activity.

Preparation of EPR Samples—Nitroxide-labeled PtdCho species, 1-acyl-2-(*n*-(4,4-dimethyloxazolidine-*N*-oxyl)stearoyl)-*sn*-glycero-3-phosphocholine (*n*-doxyl-PtdCho), with the spin label positioned at $n = 5, 7, 10, 12$, and 16, were purchased from Avanti Polar Lipids, Inc. (Alabaster, AL) (Fig. 2) as chloroform solutions. Organic solvents for calibrating high field EPR spectra for polarity and hydrogen-bonding effects included methanol, isopropyl alcohol, and hexane (Sigma). All solvents were analytical grade or higher and were used as received. Nickel(II) ethylenediamine-*N*,*N*′-diacetic acid (NiEDDA) was synthesized as described (12). NiEDDA 200 mM stock solution was prepared in lysis buffer. 5-Doxyl-stearic acid (5-doxyl-SA) was purchased from TCI America (Portland, OR). Solutions of 5-doxyl-SA were typically prepared at concentrations ≤1 mM (*i.e.* below the critical micellar concentration). A solution of 5-doxyl-PtdCho in isopropyl alcohol was prepared at 0.1 mM concentration.

Preparation of n-Doxyl-PtdCho Dispersions and n-Doxyl-PtdCho Binding to Sec14p—Multilamellar aqueous dispersions of *n*-doxyl-PtdCho (20% by weight) were prepared as described (13). Previous studies have shown that spin-labeled lipids form bilayers when dispersed in water and exhibit similar phase behavior as biological lipids (14).

To load Sec14p with *n*-doxyl-PtdCho, a 95 μM protein solution was mixed with a small molar excess of 100% spin-labeled multilamellar liposomes and incubated at room temperature for at least 2 h. As an assay for completeness of binding, we monitored binding of *n*-doxyl-PtdCho to Sec14p by X-band EPR until no further changes in the signal amplitude were observed. This assay relies on our observation that the EPR signal from an isolated spin label typically exhibits much narrower features and is easily distinguished from EPR spectra originating from *n*-doxyl-PtdCho liposomes (see "Results").

EPR Spectroscopy and Spectral Analysis—Continuous wave (CW) X-band (9.0–9.5 GHz) EPR spectra were acquired with a Century Series Varian E-109 (Varian Associates, Palo Alto, CA) EPR spectrometer and digitized to 2000 data points/spectrum. Typical spectrometer settings were as follows: microwave power 2 milliwatts, field modulation frequency 100 kHz, and amplitude less than 1 G to avoid overmodulation. Specific ranges of magnetic field scans are indicated in the figures. Variable temperature EPR spectra were obtained using a nitrogen flow system connected to a Varian variable temperature controller. Sample temperature was measured with a VWR International (West Chester, PA) digital thermometer equipped with a stainless steel microprobe positioned in the cavity just above the sample. The VWR thermometer has a resolution of 0.001 °C and accuracy of ±0.05 °C. In all experiments, temperature was controlled better than ±0.5 °C.

High field (HF) EPR spectra were acquired with a 130 GHz EPR spectrometer constructed and installed in the Argonne National Laboratory (Argonne, IL). Field-swept echo-detected EPR spectra from spin-labeled samples were recorded at a temperature of 25 K using a two-pulse sequence. Typically, $\pi/2$ pulses of 50 ns in length were separated by a 350-ns delay, and the repetition rate was set to 500 Hz. For detecting low temperature rigid limit HF EPR spectra, we employed an echo-detected field-swept mode over the conventional continuous wave scheme for several reasons. First, the pulse detection eliminates signals originating from spin-labeled *n*-doxyl-PtdCho bilayers (*i.e.* phospholipids aggregated in a solution and not bound to Sec14p), because spins of the former molecules have much shorter phase memory T_2 relaxation time due to strong magnetic interactions with the neighboring spins. Second, low temperature echo-detected HF EPR spectra do not have microwave phase distortions, allowing for more accurate line shape and *g*-factor analysis.

For HF EPR, spin-labeled samples were drawn by capillary action into clear fused quartz tubes (inner diameter = 0.5 mm, outer diameter = 0.6 mm; VitroCom, Mountain Lakes, NJ), sealed with a Critoseal clay (purchased from Fisher), and loaded

into precooled cryostat at 25 K. Temperature of the EPR resonator and the sample was controlled by an ITC-4 temperature controller coupled to a flow cryostat (all supplied by Oxford Instruments, Concord, MA).

Saturation recovery (SR) pulsed EPR experiments were conducted at 4 °C with a Bruker Biospin (Billerica, MA) X-band ElexSys 680 EPR spectrometer installed at the National High Magnetic Field Laboratory (Tallahassee, FL). The SR measurements were performed using a 0.16-μs pump pulse and an amplifier output of 10 watts. Shot repetition time was 204 μs. Each SR curve was digitized to 1024 points. Data were acquired at the field position corresponding to the maximum EPR intensity ($m_I = 0$ hydrogen hyperfine transition). Reference signal was acquired at the 50-G shift in the lower field. Data on NiEDDA accessibility to 5-doxyl-SA in a water/ethanol mixture were provided by Dr. J. Widomska (National Biomedical EPR Center, Milwaukee, WI).

Lorentzian line broadening induced by NiEDDA was measured from CW X-band spectra using a one-parameter model (13, 15, 16). In brief, first derivative EPR spectra measured in the presence of NiEDDA were least squares fitted using the Levenberg-Marquardt algorithm to a convolution of the corresponding experimental spectra recorded in the absence of paramagnetic relaxant and a Lorentzian broadening function. A modification of this approach for elucidating very small broadening effects has been described (17).

RESULTS

Binding of n-Doxyl-PtdCho to Sec14p—Binding of *n*-doxyl-PtdCho to Sec14p was monitored from changes in EPR spectra collected at room temperature. Fig. 3*A* (*dots*) shows a typical room temperature EPR signal obtained for 5-doxyl-PtdCho liposomes. For all *n*-doxyl-PtdCho species studied, the signal appeared as a single line of ~25–27 G peak-to-peak width. Such a spectrum is characteristic of strong dipole-dipole and exchange interactions.

The single line EPR spectrum of spin-labeled lipids is well modeled by a Lorentzian function as illustrated for 5-doxyl-PtdCho in Fig. 3*A*; least squares simulations are shown as a *solid line* that very closely follows the experimental spectrum. The spectrum in Fig. 3*A* also demonstrates that the EPR signals from nonaggregated *n*-doxyl-PtdCho (*i.e. n*-doxyl-PtdCho resident in the aqueous buffer) are too weak to be detected under these conditions. This is expected, because the critical micelle concentration for *n*-doxyl-PtdCho is in the nanomolar range, resulting in a concentration of *n*-doxyl-PtdCho monomers in aqueous buffer that is well below the typical sensitivity of X-band EPR spectrometers.

When Sec14p loads with a phospholipid from a membrane bilayer, the bound phospholipid becomes encapsulated in the protein cavity. Such a loading event effectively eliminates spin-spin interactions for the bound *n*-doxyl-PtdCho and produces significant line shape changes. Fig. 3*B* (*solid line*) depicts a typical EPR spectrum observed in experiments where Sec14p was mixed with multilamellar 5-doxyl-PtdCho bilayers and allowed to equilibrate for ~2 h. A sharp decrease in spin-spin interactions was observed for Sec14p-bound 5-doxyl-PtdCho as reported by the line narrowing.

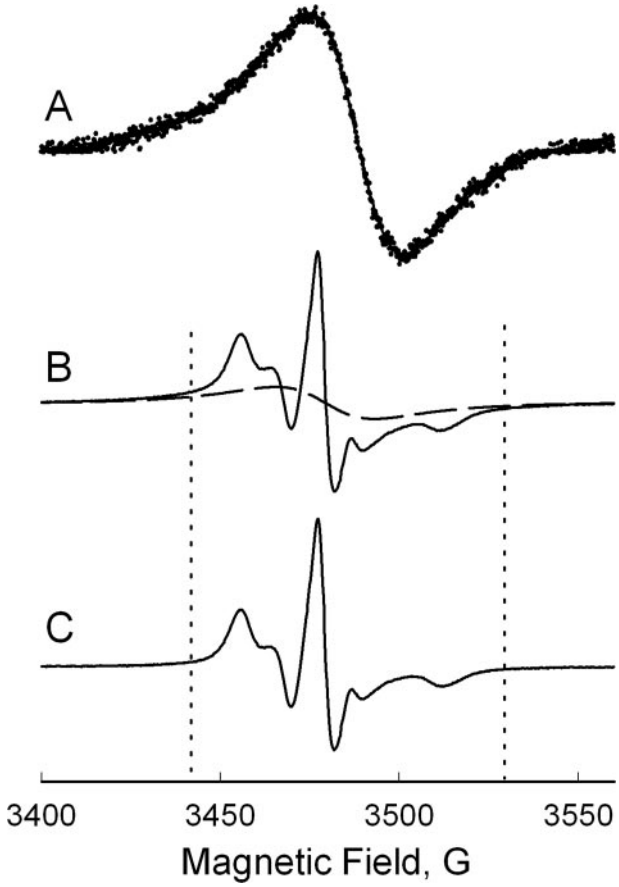

FIGURE 3. **Room temperature X-band CW EPR spectra from 5-doxyl-PtdCho.** *A*, in a form of multilamellar lipid dispersion (field modulation amplitude 8G) (*B*, *solid line*) after mixing with 95 μM Sec14p in ~1:1 molar ratio. Least squares fit of the spectrum (*A*) to a Lorentzian function is shown as a *dashed line* (*B*). *C*, signal from *5*-doxyl-PtdCho incorporated into the Sec14p binding pocket obtained by the spectral subtraction.

This line narrowing results in a significant (~6-fold) increase in the peak-to-peak amplitude of the corresponding EPR spectrum as compared with the initial signal from liposomal *5*-doxyl-PtdCho. The presence of the signal from aggregated lipids is particularly noticeable from broad wings that extend far away from characteristic features (*i.e. outside* the *dashed lines* in Fig. 3*B*). Thus, the signal from Sec14p-bound *5*-doxyl-PtdCho dominates the first derivative EPR spectrum observed in CW experiments, thereby simplifying initial analyses of local spin label dynamics. In time domain experiments, such as saturation recovery and echo-detected field-swept HF EPR, little if any contribution from the liposomal *5*-doxyl-PtdCho is recorded, because the latter spin species have much shorter electronic relaxation times. However, for accurate line shape least squares simulation analyses, the contribution from the remaining liposomal 5-doxyl-PtdCho (*dashed line*) is subtracted from the experimental spectrum (Fig. 3*B*, *solid line*), yielding the Sec14p-bound 5-doxyl-PtdCho spectrum (Fig. 3*C*). In this particular experiment, the fraction of liposomal *5*-doxyl-PtdCho molecules was determined to be ~30%.

Local Dynamics of n-Doxyl-PtdCho Incorporated into the Sec14p Phospholipid Binding Pocket—The data described above demonstrate that Sec14p loads with *n*-doxyl-PtdCho and

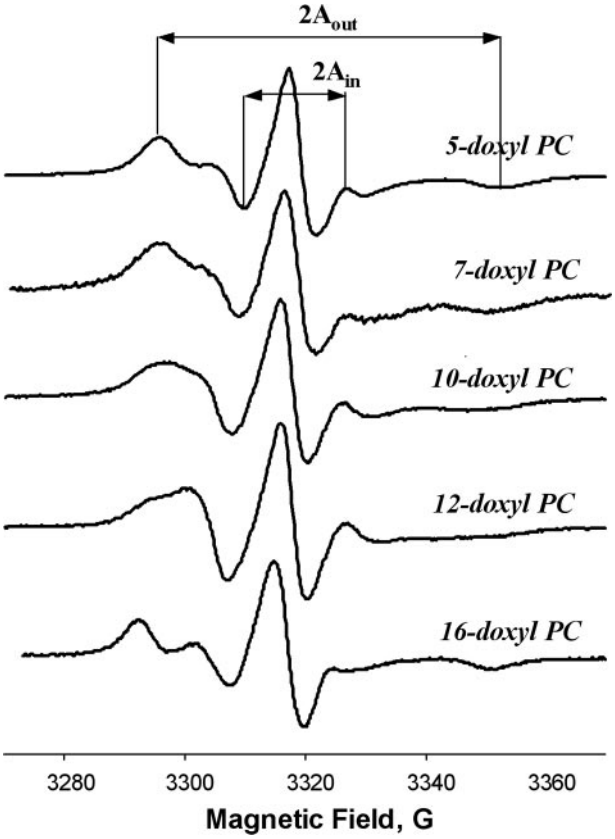

FIGURE 4. **Room temperature X-band CW EPR spectra from Sec14p-bound *n*-doxyl-PtdCho.** Spectra are corrected for the background signal as illustrated in Fig. 2 and are intensity-normalized using double integration.

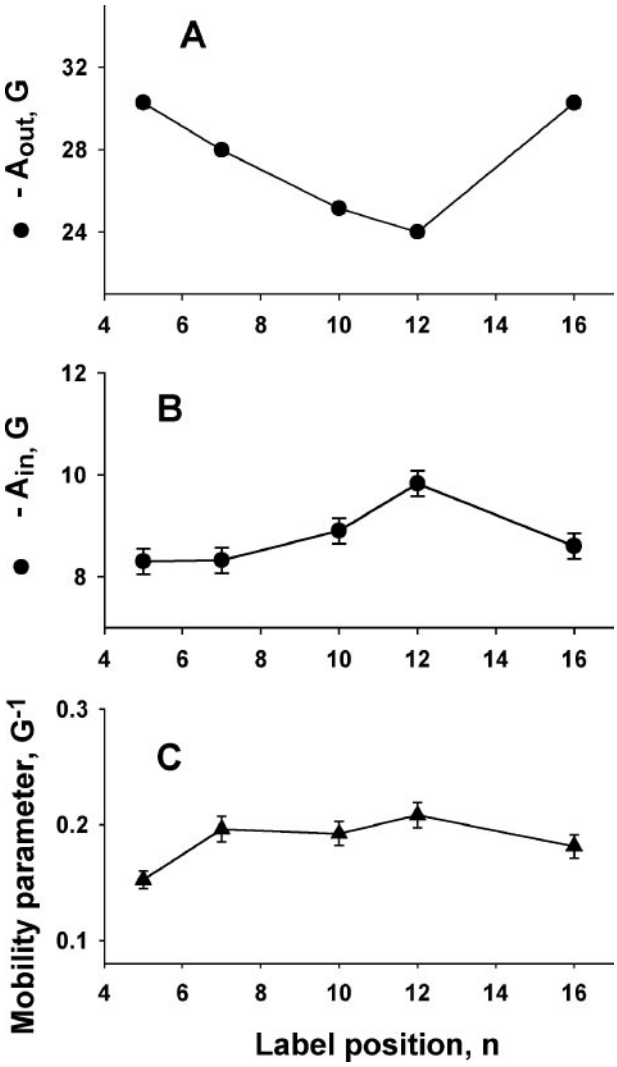

FIGURE 5. **Empirical motional characteristics of nitroxide spin label as determined from room temperature T = 22 °C X-band CW EPR spectra of *n*-doxyl-PtdCho bound to Sec14p as function of the label position along the *sn*-2 acyl chain.** *A*, A_{out}; *B*, A_{in}; *C*, mobility parameter, $\Delta H_{p\text{-}p}^{-1}$ ($m_I = 0$).

that the bound *n*-doxyl-PtdCho becomes sequestered within the protein cavity. Since CW EPR spectra of spin-labeled phospholipids are sensitive to rotational motion of the nitroxide moiety, this method was used to investigate the flexibility of the *n*-doxyl-PtdCho acyl chain within the Sec14p lipid binding pocket. A series of room temperature (22 °C) CW X-band spectra from *n*-doxyl-PtdCho (where $n = 5, 7, 10, 12$, and 16) bound to Sec14p are shown in Fig. 4. For all label positions analyzed, the contribution of liposomal *n*-doxyl-PtdCho registered only as a broad line most readily observed at the wings. This component was subtracted from experimental spectra and will not be discussed further. Instead, we focus on the dominant EPR spectrum that originates from *n*-doxyl-PtdCho sequestered within the Sec14p cavity.

All EPR spectra depicted in Fig. 4 report an intermediate to slow motional regime and anisotropic rotation of the nitroxide spin label. The absence of any abnormal broadening and/or substantial drop in intensity of these spectra indicative of spin-spin interactions is consistent with a Sec14p molecule loading with a single *n*-doxyl-PtdCho molecule. A particularly informative parameter of such spectra is the peak-to-peak width $\Delta H_{p\text{-}p}$ ($m_I = 0$) of the central nitrogen hyperfine component (where $m_I = 0$ is the nitrogen spin quantum number). When tumbling of a spin label falls into an intermediate to slow motional regime, this width is approximately proportional to the rotational correlation time τ_c. In studies of local dynamics of protein side chains, an inverse of this width $\Delta H_{p\text{-}p}^{-1}$ ($m_I = 0$) is typically reported as a "mobility" parameter (18). This parameter reliably estimates mobility of spin-labeled amino acid side chains in proteins, and a smaller mobility parameter indicates slower rotation and a longer rotational correlation time τ_c. Other useful parameters for characterizing rotational tumbling of a nitroxide are the effective hyperfine splitting constants A_{out} and A_{in} as defined in Fig. 4. A plot of the mobility parameter, $\Delta H_{p\text{-}p}^{-1}$ ($m_I = 0$), as well as A_{out} and A_{in}, all indicate a progressive increase in spin label local mobility as the nitroxide label is moved toward the headgroup-distal end of the *sn*-2 acyl chain from position C_5 to C_{12} (Fig. 5). At position C_{16}, however, motion of the label becomes more restricted, very much like at position C_5. We used the definition of McConnell and Hubbell to calculate the effective order parameter (S^{eff}) to describe the anisotropy of spin label motion (19, 20),

$$S^{eff} = \frac{(A_{\parallel} - A_{\perp})A_0}{\frac{1}{3}(A_{\parallel} + 2A_{\perp})\Delta A} \qquad \text{(Eq. 1)}$$

where $A_{\parallel} = A_{out}$ (*i.e.* a half of the outer hyperfine splitting), and

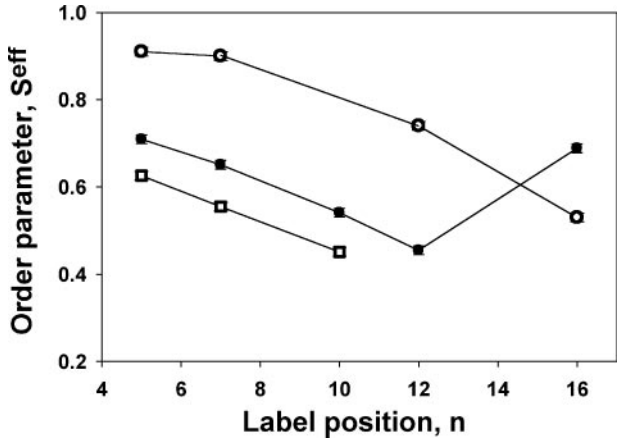

FIGURE 6. **Effective order parameters S^{eff} calculated from X-band CW EPR spectra as a function of the label position.** *Filled circles*, *n*-doxyl-PtdCho bound to Sec14p (T = 27 °C); *open circles*, S^{eff} for *n*-doxyl-PtdCho in dimyristoyl-PtdCho bilayers in a crystalline phase (T = 5 °C); *open squares*, S^{eff} for *n*-doxyl-PtdCho in dimyristoyl-PtdCho bilayers in fluid phase (T = 27 °C)

$A_\perp$ is calculated from A_{in}, a half of the inner hyperfine splitting expressed in gauss,

$$A_\perp = (A_{in} + 0.85) \quad \text{for} \quad S^{app} < 0.45 \qquad \text{(Eq. 2)}$$

$$A_\perp = A_{in} + 1.32 + 1.86 \log(1 - S^{app}) \quad \text{for} \quad S^{app} > 0.45 \qquad \text{(Eq. 3)}$$

$$S^{app} = (A_{out} - A_{in})/\Delta A \qquad \text{(Eq. 4)}$$

where A_0 is the isotropic nitrogen hyperfine coupling constant, and ΔA is the maximum extent of the axial nitrogen hyperfine anisotropy (21, 22). Although the values of ΔA and A_0 vary by a few percent with the position of the label along the *sn*-2 acyl chain of Sec14p-bound *n*-doxyl-PtdCho, we found it convenient to fix A_0 and ΔA for all *n*-doxyl-PtdCho isomers to those values observed for 5-doxyl-PtdCho in isopropyl alcohol. In doing so, we introduced less than 3% error into the S^{eff} calculations. Effective order parameters S^{eff} calculated from room temperature X-band EPR spectra of Sec14p-bound *n*-doxyl-PtdCho are reported in Fig. 6 and are compared with S^{eff} values measured for *n*-doxyl-PtdCho in either a fluid dimyristoyl-PtdCho membrane bilayer environment (T = 27 °C) or in a crystalline bilayer environment (T = 5 °C).

Substantial alterations in the label dynamic and order parameters are recorded as a function of the spin label position along the *sn*-2 acyl chain. Qualitative analyses of EPR spectra for Sec14p-bound 5-doxyl-PtdCho indicate a highly restricted "slow motional" regime that corresponds to $\tau_c \approx 6-10$ ns. For this position, the mobility parameter is the lowest ($\Delta H_{p\text{-}p}^{-1}$ = 0.15 G^{-1}), whereas the order parameter is the highest (S^{eff} = 0.72). For 7-doxyl-PtdCho, the mobility parameter increases to $0.22G^{-1}$, whereas S^{eff} decreases to 0.66. The outer hyperfine splitting A_{out} parameter decreases to 28 G, whereas A_{in} remains essentially the same. Such changes indicate faster and less anisotropic local tumbling of the label that is consistent with an increased local flexibility of the *sn*-2 acyl chain at C_7 relative to C_5. For 10-doxyl-PtdCho, the mobility parameter remains essentially the same, but A_{out} reduces to 25.15 G, and the order parameter decreases to S^{eff} = 0.56. This indicates reduced anisotropy of motion. For 12-doxyl-PtdCho, anisotropy of motion is diminished even further, and the nitroxide tumbling becomes even faster as reported by the increased mobility parameter.

These collective data indicate an increase in *sn*-2 acyl chain rotational flexibility with increased distance from the headgroup/backbone-proximal region of the Sec14p-bound PtdCho molecule and support a model where Sec14p engages bound PtdCho most tightly at the backbone-headgroup and backbone-proximal regions of the phospholipid molecule. The data obtained for the series of *n*-doxyl-PtdCho molecules where the nitroxide is positioned at and between C_5 and C_{12} are consistent with this hypothesis. The spectrum for 16-doxyl-PtdCho is defined by the outer peaks separated by A_{out} = 30.27 G and has an order parameter S^{eff} = 0.71. Those values report a very strong immobilization of the nitroxide label and compare favorably with parameters measured for 5-doxyl-PtdCho. The abrupt change in the mobility trend suggests that the tail of the lipid is stacked against the "floor" of the protein cavity. It is also possible that Sec14p is capable of forming hydrogen bond contacts with the somewhat hydrophilic nitroxide group of 16-doxyl-PtdCho.

PtdCho Is Strongly Immobilized in the Sec14p Phospholipid Binding Pocket—Although a progressive increase in chain mobility in the direction from the lipid head to the tail up to position C_{12} is clear from the EPR spectra described above, variable temperature EPR experiments demonstrate that the local motion of the Sec14p-bound PtdCho *sn*-2 acyl chain remains highly restricted (Fig. 7). At all temperatures, all X-band EPR spectra for *n*-doxyl-PtdCho molecules labeled at positions C_5, C_7, and C_{10} report a single component. Analyses of these spectra indicate a gradual decrease in the spectral anisotropy and an increase in mobility parameter, $\Delta H_{p\text{-}p}^{-1}$, with increased temperature.

The activation energies associated with these dynamic processes were calculated by plotting EPR spectral parameters as a function of temperature in the Arrhenius coordinates (Fig. 8). For 5-doxyl- and 7-doxyl-PtdCho molecules, the slopes of the linear regressions were essentially the same (-1.48×10^3 K^{-1} and -1.47×10^3 K^{-1}, respectively) yielding an activation energy of E_a = 12.3 kJ mol^{-1}. For 10-doxyl-PtdCho, however, the slope changes to -0.85×10^3 K^{-1} (E_a = 7.1 kJ mol^{-1}), indicating that the molecular interactions responsible for the binding interface between bound PtdCho and Sec14p differ along the *sn*-2 acyl chain. Specifically, the effective potential barrier in the vicinity of the headgroup/backbone-proximal region of the Sec14p-bound PtdCho is greater than for the distal regions of the *sn*-2 acyl chain.

Pulse Saturation EPR Analysis of Accessibility of Sec14p-bound n-Doxyl-PtdCho to a Soluble Broadening Agent—To probe how PtdCho is oriented within the Sec14p binding pocket, we measured the accessibility of the nitroxide spin label in a series of Sec14p-bound *n*-doxyl-PtdCho molecules to water-soluble paramagnetic broadening reagent (NiEDDA). An analogous approach has proven to be informative in determination of local protein folds and transmembrane protein structure (23–32) and for mapping structural elements of membrane and peripheral proteins (25, 26). Moreover, the accessibility parameters of protein side chains measured by

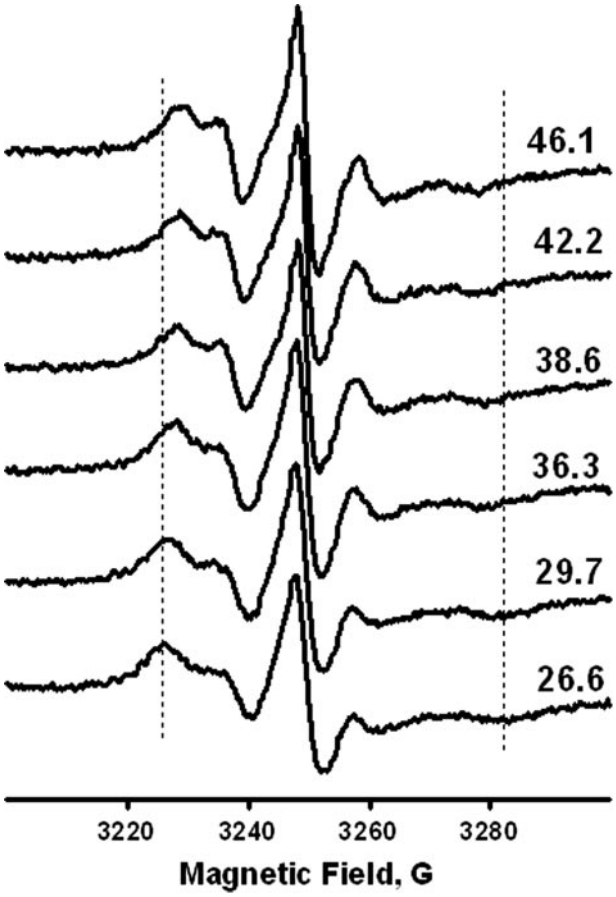

FIGURE 7. **Variable temperature intensity-normalized experimental 9.5 GHz CW EPR spectra from *5*-doxyl-PtdCho bound to Sec14p.**

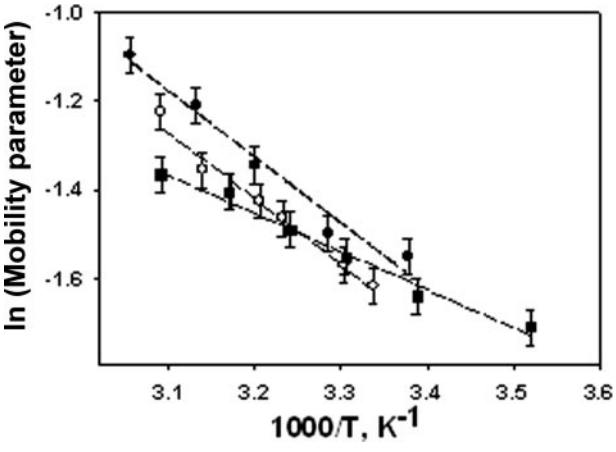

FIGURE 8. **Temperature dependence of the mobility parameter for *n*-doxyl-PtdCho bound to Sec14p plotted in Arrhenius coordinates.** *Open circles*, *5*-doxyl-PtdCho; *filled circles*, *7*-doxyl-PtdCho; *filled squares*, 10-doxyl-PtdCho. Best fit to the linear regression is shown as *dashed lines*.

EPR agree well with those computed from crystal structures (23, 24).

The accessibility parameter is proportional to the Heisenberg exchange frequency (W_{ex}) of a nitroxide label with a broadening agent that is freely diffusing in a solution. For the broadening agent employed, the electronic spin-lattice relaxation time is much shorter than that of a nitroxide, and the Heisenberg spin exchange is the predominant spin-spin interaction that affects both spin label electronic relaxation times (T_1 and T_2).

Initially, molecular accessibility of the *sn*-2 acyl chain of Sec14p-bound *n*-doxyl-PtdCho was accessed in pulsed SR EPR experiments to measure spin label electronic T_{1e} directly in the absence and presence of NiEDDA (50 mM). The amplitude of SR EPR signals observed for the central ($m_I = 0$) nitrogen hyperfine component in the absence (I) and the presence (I^{relaxant}) of a paramagnetic relaxant can be described as follows,

$$I = A_{10} + A_1(1 - e^{-R_{1e}t}) \quad \text{(Eq. 5)}$$

$$I^{\text{relaxant}} = A_{20} + A_2(1 - e^{-R_{1e}^{\text{relaxant}}t}) \quad \text{(Eq. 6)}$$

where R_{1e} and R_{1e}^{relaxant} are the corresponding electronic spin-lattice relaxation rates. The difference in the relaxation rates R_{1e} and R_{1e}^{relaxant} is proportional to the local concentration of the relaxant,

$$\Delta R = R_{1e}^{\text{relaxant}} - R_{1e} = \chi[\text{relaxant}] \quad \text{(Eq. 7)}$$

where the relaxivity constant χ is in turn proportional to the relative translational diffusion rate (D), which is the sum of translational diffusion rates of the spin label and the relaxant (D^{SL} and D^{relaxant}, respectively). Other contributing factors are the efficiency (ρ) of a given collision to produce additional relaxation of the nitroxide spin and the collision distance r,

$$\chi = 4\pi r\rho(D^{\text{SL}} + D^{\text{relaxant}}) \quad \text{(Eq. 8)}$$

The difference in relaxation rates (ΔR) for a given relaxant is a time-domain analogue of the accessibility parameter Π derived from CW EPR experiments (13, 33, 34).

Under the experimental conditions employed herein, the rotational correlation time τ_c of the spin label falls within the 1–10 ns range, whereas the typical nuclear relaxation time for nitroxides is ~100 ns (34). Thus, recovery of the signal due to such fast processes is complete within EPR detection dead time and does not contribute to the SR EPR signal. Similarly, *n*-doxyl-PtdCho molecules remaining in an aggregated form (*i.e.* not associated with Sec14p) and therefore experiencing strong spin-spin interactions exhibit electronic spin label relaxation rates that are much faster than those recorded for *n*-doxyl-PtdCho molecules loaded into the Sec14p phospholipid binding cavity. Consequently, signals from these irrelevant sources do not contribute to the observed SR signal.

For solvent-exposed nitroxide labels, the exchange rate (W_{ex}) with NiEDDA clamped at a concentration of 50 mM is expected to be $W_{ex} \approx 10^5\ s^{-1}$, whereas the electronic relaxation rate R_{1e} is $\sim 10^6\ s^{-1}$. Therefore, for a single-component EPR spectrum, one expects to observe a monoexponential SR EPR signal. Experimental SR curves recorded in the absence and presence of NiEDDA were fitted with a single or a double exponential function. Fig. 9 shows the first 4-μs profile of a typical SR EPR signal measured for air-equilibrated samples of Sec14p-bound 5-doxyl-PtdCho with and without NiEDDA challenge. Since mechanisms of electronic relaxation through Heisenberg spin exchange for paramagnetic oxygen and NiEDDA are statistically independent and are not cross-correlated, the effect of

oxygen is additive and included in R_{1e}. Both curves are well modeled by a single exponential function, confirming that SR EPR signals from any aggregated 5-doxyl-PtdCho still present in this sample are invisible in the pulse saturation EPR experiment. SR EPR relaxation data are summarized in Table 1. For Sec14p-bound 5-doxyl-PtdCho, the electronic relaxation rates in the absence and presence of 50 mM NiEDDA were very similar (1.10 ± 0.01 and 1.14 ± 0.02 MHz, respectively). These data indicate that the C_5 position of the *sn*-2 acyl chain of Sec14p-bound 5-doxyl-PtdCho is essentially inaccessible to NiEDDA.

For 16-doxyl-PtdCho, the relaxation rate has changed from $R_{1e} = 0.41$ MHz in the absence of relaxant to $R_{1e}^{\text{relaxant}} = 1.78$ MHz, corresponding to an increase in relaxation rate by $\Delta r = 1.37$ MHz in the presence of 50 mM NiEDDA (*i.e.* by 0.027 MHz/mM NiEDDA).

To evaluate to what degree binding to Sec14p shields *n*-doxyl-PtdCho from collision with the hydrophilic NiEDDA complex, we measured the relaxivity parameter χ for an unshielded (*i.e.* unbound) lipid. To overcome problems posed by the insolubility of *n*-doxyl-PtdCho in water, we utilized a structurally similar compound, 5-doxyl-stearic acid (5-doxyl-SA), dissolved in a 50%/50% (v/v) water-ethanol mixture as a reporter. In the presence of 20 mM NiEDDA, χ was 0.15 MHz/mM. Corrections for the differences in relative translational diffusion rate of 5-doxyl-SA and the relaxant were evaluated using a simple hydrodynamic model for $D = kT/6\pi\eta r$, where η is the viscosity of the solution and r is the hydrodynamic radius of the molecule. In these simplified calculations, we assume the encounter partners are spherical in shape. For the spin label bound to the protein, the nitroxide translational diffusion coefficient becomes that of the protein itself and is negligible compared with D^{relaxant}. Thus, we can assume that $(D^{\text{SL}} + D^{\text{relaxant}}) = D^{\text{relaxant}}$ in Equation 8. The collision distance r remains the same, since NiEDDA and a nitroxide, but not the protein itself, are the colliding species. For 5-doxyl-SA and NiEDDA, the hydrodynamic radii are taken to be approximately the same, resulting in $(D^{\text{SL}} + D^{\text{relaxant}}) = 2D^{\text{relaxant}}$. Assuming that the collision efficiency ρ does not vary with solvent, the relationship between the relaxivity χ' observed for spin-labeled protein in an aqueous solution of viscosity η' and the relaxivity χ'' for an unbound label in a water-ethanol mixture of viscosity η'' is $\chi'/\chi'' = \eta''/2\eta'$. Adjusting for the differences in viscosities of the solutions (35), the ratio χ'/χ'' is estimated to be ~1.43. Based on this calculation, we estimate the relaxivity for an unshielded doxyl label bound to protein to be 0.22 MHz/mM NiEDDA. The accessibility to the specific protein site is calculated as a ratio of the experimentally observed relaxivity to the relaxivity of the model unshielded site (0.22 MHz/mM NiEDDA). For Sec14p-bound 5-doxyl-PtdCho, the relaxant accessibility is ~0.4%, whereas for 16-doxyl-PtdCho, it is ~13%.

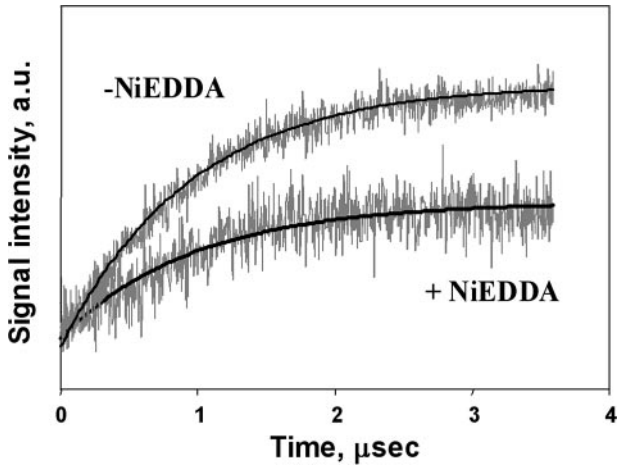

FIGURE 9. **First 4 μs of saturation recovery signal from 5-doxyl-PtdCho bound to Sec14p in the absence and in the presence of 50 mM NiEDDA at T = 4 °C.** Best fit to the single exponential growth is shown as a *solid line*.

Comparisons of the effects of NiEDDA on the electronic relaxation of Sec14p-bound *n*-doxyl-PtdCho with those reported for unshielded, solvent-exposed labeled sites are informative. For solvent-exposed side chains of water-soluble proteins labeled with 1-oxyl-2,2,5,5-tetramethyl-3-pyrroline-3-methyl (MTSL), ΔR is typically about 0.13–0.22 MHz/mM NiEDDA (36). Although the effectiveness of collisions between NiEDDA and the *n*-doxyl-PtdCho spin label could differ from collisions of NiEDDA with MTSL, the largest χ value we observed (0.027 MHz/mM for 16-doxyl-PtdCho) is still substantially lower than those measured for water-exposed protein residues. We have also compared our χ values with those of transmembrane helices. For example, Robinson and co-workers (37) investigated the effects of NiEDDA on electronic relaxation of an MTSL-labeled transmembrane WALP peptide incorporated into 1,2-dioleoyl-*sn*-glycero-3-phosphocholine bilayers. For a spin-labeled site located ~10 Å from the center of the bilayer, χ was measured to be 0.0006 MHz/mM, whereas at a site positioned closer to the membrane surface (18 Å from the bilayer center), χ was recorded at 0.0016 MHz/mM. The $\chi = 0.0008$ MHz·mM^{-1} value we measure for Sec14p-bound 5-doxyl-PtdCho falls between these two values.

Collectively, the ΔR value obtained for Sec14p-bound 5-doxyl-PtdCho by pulse saturation EPR methods indicates that C_5 of the *sn*-2 acyl chain exhibits a solvent molecular inac-

TABLE 1

Accessibility of lipid-labeled sites as measured in saturation recovery EPR experiments

Concentration of NiEDDA in each experiment was 50 mM unless otherwise specified. The χ' values are corrected χ values when viscosity is taken into consideration. ΔR_{1e} and χ values for shielded and unshielded MTSL-labeled sites challenged with NiEDDA were reported elsewhere (36, 37). Accessibility of the each specified nitroxide spin label is calculated as the ratio of $\chi/\chi' \times 100\%$, as indicated.

	R_{1e}^{O}	R_{1e}^{R}	ΔR_{1e}	χ	χ' (corrected)	Accessibility ($\chi/\chi' \times 100\%$)
	MHz	*MHz*	*MHz*	*MHz/mM*	*MHz/mM*	*%*
5-Doxyl-PtdCho (Sec14p-bound)	1.10	1.14	0.04	0.0008		0.4
16-Doxyl-PtdCho (Sec14p-bound)	0.41	1.78	1.37	0.027		13
5-Doxyl-SA (water/EtOH, 20 mM NiEDDA)			3.0	0.15	0.22	
Shielded MTSL site			0.08		0.0016	
Unshielded MTSL site			0.4–0.6		0.13–0.22	

TABLE 2

Accessibility of lipid-labeled sites as measured in X-band CW EPR experiments

Concentration of NiEDDA is 50 mM in all experiments. $\delta\Delta H_{p\text{-}p}$ for 5-doxyl-SA was measured in a water/EtOH solution (1:1, v/v). This measurement represents a model "unshielded" nitroxide label. The $\delta\Delta H'_{p\text{-}p}$ value corrected for viscosity of the water/EtOH solution is also given. Accessibility of the each specified nitroxide spin label is calculated as the ratio of $\delta\Delta H_{p\text{-}p}/\delta\Delta H'_{p\text{-}p} \times 100\%$, as indicated.

	$\delta(\Delta H_{p\text{-}p})$	$\delta(\Delta H_{p\text{-}p})$	$\delta(\Delta H_{p\text{-}p})'$ (corrected)	Accessibility ($\delta\Delta H/\delta\Delta H' \times 100\%$)
	mG	*mG/mM*	*mG/mM*	*%*
5-Doxyl-PtdCho (Sec14p-bound)	90	1.8		6
10-Doxyl-PtdCho (Sec14p-bound)	90	1.8		6
12-Doxyl-PtdCho (Sec14p-bound)	100	2.0		7.4
16-Doxyl-PtdCho (Sec14p-bound)	310	6.2		23
5-Doxyl-SA (water/EtOH)		19	27	

cessibility comparable with that of a deeply buried protein site. However, experiments with Sec14p-bound 16-doxyl-PtdCho reveal that ΔR for the C_{16} position of that acyl chain is measurably higher, suggesting that C_{16} is a partially shielded site with a solvent accessibility ~13% that of an unshielded label.

CW EPR Analysis of Accessibility of Sec14p-bound n-Doxyl-PtdCho to NiEDDA—To complement the SR EPR data, we employed CW EPR to evaluate accessibility of spin label to NiEDDA in a series of *n*-doxyl-PtdCho molecules loaded into Sec14p. Collisions between a label and a paramagnetic relaxant shorten the nitroxide electronic T_2 relaxation time. This effect is observed as Lorentzian broadening that is uniform across the experimental CW EPR spectrum. Detailed investigations of nitroxide-NiEDDA spin-spin interactions in solutions of various viscosities (η) demonstrate that collisions are in a "strong" exchange limit and that Lorentzian broadening induced by NiEDDA is a linear function of $1/\eta$ up to NiEDDA concentrations of 100 mM (25). The contribution to the line width from dipolar spin-spin interactions is negligible.

The data collected from CW EPR measurements of the peak-to-peak Lorentzian broadening in the presence and absence of NiEDDA (50 mM) are summarized in Table 2. Lorentzian broadening was extracted using a one-parameter convolution algorithm (15). The broadening was determined to be only 90 mG (measured as peak-to-peak) for Sec14p-bound 5-doxyl-PtdCho and 10-doxyl-PtdCho. This value is at the detection limit of the experiment. This miniscule effect is consistent with the very low accessibility of the C_5 position of the *sn*-2 acyl chain to NiEDDA as determined by the SR measurements described above. The broadening observed for 12 and 16-doxyl-PtdCho is 100 and 310 mG, respectively. Fig. 10 shows the result of the fit for 16-doxyl-PtdCho. The absence of any substantial residual of the fits confirms that the shortening of the electronic relaxation time recorded by SR EPR upon NiEDDA challenge primarily reports exchange interactions rather than changes in the dynamics of Sec14p-bound *n*-doxyl-PtdCho or significant conformational changes within Sec14p.

In a control experiment, the Lorentzian broadening for 5-doxyl-SA (1 mM) in a water/ethanol solution was measured as a function of NiEDDA concentration. The relaxivity was determined to be 19 mG/mM. When corrected for viscosity of the water/methanol mixture and for the mutual diffusion coefficient (as discussed above for SR EPR experiments), the broadening for an unprotected protein site exposed to aqueous NiEDDA was calculated to be 27 mG/mM. From this calibration, the molecular accessibility of the spin label for Sec14p-bound 16-doxyl-PtdCho is estimated to be ~23% that of an unshielded site (Table 2).

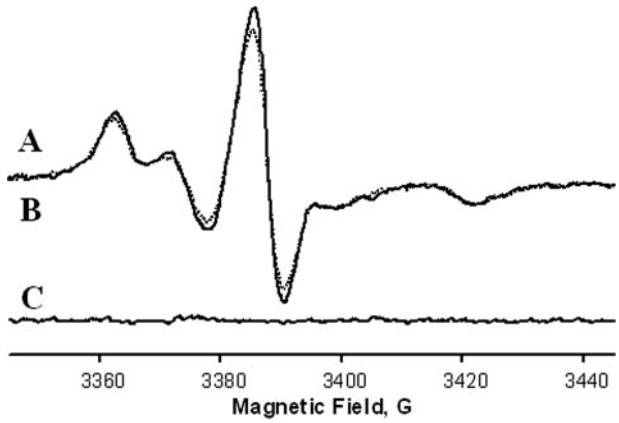

FIGURE 10. **Experimental 9 GHz CW EPR spectrum from 16-doxyl-PtdCho bound to Sec14p in the presence of 50 mM NiEDDA (*trace A, solid line*) is superimposed with the result of the fit using a Lorentzian broadening model (*trace B, dashed line*).** Residual of the fit (experiment fit) is shown as *trace C*.

In summary, the CW line width broadening accessibility data are in qualitative agreement with the SR EPR data. Both methods characterize the C_5 position of the *sn*-2 acyl chain of Sec14p-bound PtdCho as essentially inaccessible to hydrophilic NiEDDA and assign the C_{16} position of that acyl chain as a shielded, but partially accessible, site. The difference in the absolute numbers reported by SR EPR and CW measurements could be due to substantial nonhomogeneity of the labeled sites. The CW line width broadening method is sensitive only to the states with relatively high accessibility. The SR method, especially when very high concentrations of a broadening agent are used, can report on highly protected protein sites. We speculate that those two methods may be sensing conformational fluctuations of the Sec14p-PtdCho complex in solution, and that a probe positioned at the end of the *sn*-2 acyl chain is especially sensitive to such fluctuations.

Characterization of Local Polarity of the Sec14p Lipid Binding Pocket—The local polarity within the Sec14p phospholipid-binding pocket was evaluated by measuring both the electronic *g*-matrix and nitrogen hyperfine coupling tensor *A* parameters of Sec14p-bound *n*-doxyl-PtdCho species. High spectral resolution achieved by HF EPR permits very accurate determination of electronic *g*-matrix components from the powder pattern spectra and evaluation of polarity and hydrogen bond effects in a variety of biological systems (38–45).

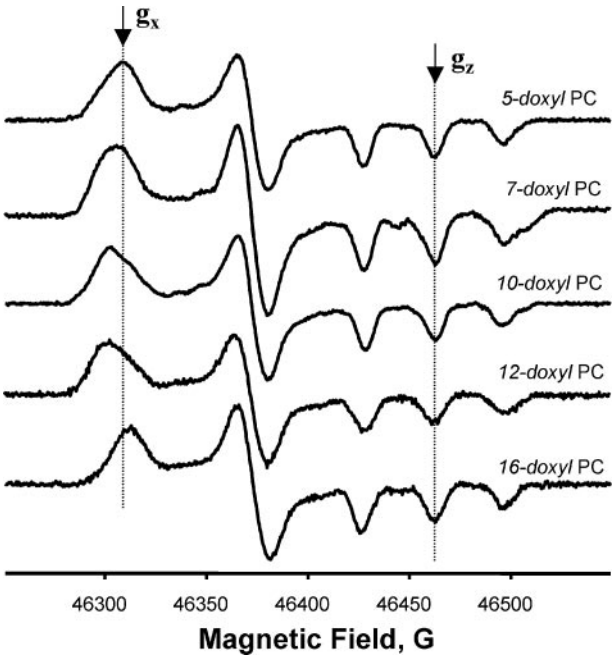

FIGURE 11. **Rigid limit 130 GHz echo-detected EPR spectra from *n*-doxyl-PtdCho bound to Sec14p at T = 25 K.**

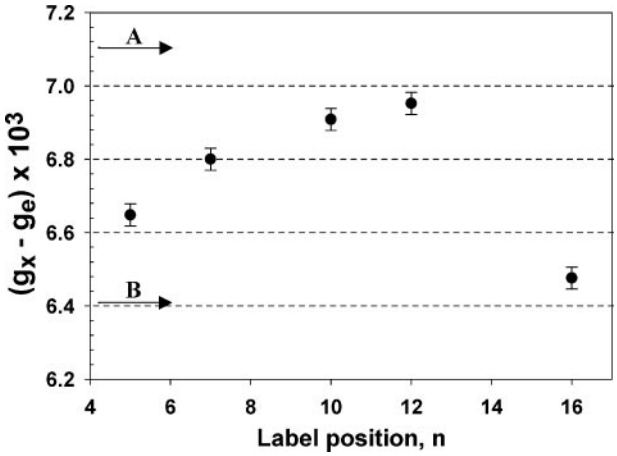

FIGURE 12. **Dependence of the g_x component on spin label chain position (*n*) for *n*-doxyl-PtdCho bound to Sec14p as measured from 130 GHz echo-detected EPR spectra.** For purposes of calibration, the *arrows* show the g_x component for *n*-doxyl-PtdCho dispersed in hexane (*A*) and in methanol (*B*).

Fig. 11 depicts a series of 130 GHz echo-detected spectra of Sec14p-bound *n*-doxyl-PtdCho. Systematic changes, primarily in magnetic field positions of the g_x (low field) spectral component, are clearly apparent. As the nitroxide label is moved from position C_5 to C_{12} of the *sn*-2 acyl chain, this component progressively shifts to a lower field. This corresponds to an increase in the magnitude of g_x. The *z*-component of the nitrogen hyperfine coupling tensor (A_z) was measured from a characteristic splitting in the high field region of the spectra. The largest values for A_z were recorded for Sec14p-bound 5-doxyl- and 7-doxyl-PtdCho, and those values were equivalent ($A_z = 34.7 \pm 0.25$ G). Those data indicate a similar polarity and proticity of the microenvironments at positions C_5 and C_7 of the *sn*-2 acyl chain of Sec14p-bound 5-doxyl- and 7-doxyl-PtdCho species. Values for A_z decreased to 33.85 ± 0.25 G for Sec14p-bound 10-doxyl-PtdCho and increased to 34.15 ± 0.25 and 35.17 ± 0.25 G for 12-doxyl-PtdCho and 16-doxyl-PtdCho, respectively. These data show small, but clearly measurable, shifts to a less polar and more aprotic environment as the spin label is positioned further down the *sn*-2 acyl chain from the headgroup/backbone region of Sec14p-bound PtdCho up to position C_{12} and return to a more polar, proctic environment at position C_{16}.

Fig. 12 shows the g_x component of electronic *g*-matrix for Sec14p-bound *n*-doxyl-PtdCho as a function of the position of the spin label along the *sn*-2 acyl chain. A systematic shift in the *x*-component to lower field/higher *g*-factor is clearly observed as the spin label is positioned along the *sn*-2 acyl chain from C_5 toward C_{12}. This trend is broken at position C_{16}, for which the g_x component shifts to higher field/lower g-factor. The observed shift indicates a transition from a polar and more protic environment at C_5 to one that is less polar and more aprotic at C_{12} and then a return to a more polar and protic environment at position C_{16}. Again, this is in agreement with our conclusions reached from measurements of the nitrogen hyperfine coupling component A_z. On the other hand, the g_y component was insensitive to spin label position. This is consistent with both theoretical and experimental considerations that the *y*-component of electronic *g*-matrix is much less affected by solvent polarity than is the *x*-component (39–41).

Polarity Reference Measurements—As a means for calibrating polarity references for *n*-doxyl-PtdCho, we obtained 130 GHz spectra from 5-doxyl-PtdCho dispersed in methanol, isopropyl alcohol, and hexane. Analysis of g_x and A_z magnetic parameters as a function of the label position *n* on the *sn*-2 acyl chain indicated that C_5 and C_{16} were situated in the most polar protic environment. The local polarity gradually changes to less polar and more aprotic as the label is moved along the *sn*-2 acyl chain to C_{12}. From comparisons of 130 GHz EPR spectra of Sec14p-bound *n*-doxyl-PtdCho with those measured for 5-doxyl-PtdCho in these organic solvents, we find that the local electrostatic environment of C_5 and C_7 approximates that of bulk isopropyl alcohol. For comparison, g_x for spin label in hexane is also shown (Fig. 12).

In principle, the observed shift might have two origins. The first one is the effect of hydrogen bond formation, and the second is the effect of polar amino acid side chains located in the immediate vicinity of the label. Previous studies have shown that the g_x shift is substantially higher in protic solvents capable of hydrogen bond formation than in aprotic solvents, even if the solvents have comparable dielectric constants (43). Theoretical analyses using density functional theory (DFT) calculations predicted that formation of a single hydrogen bond would shift the g_x component by $\Delta g_x = -4.4 \times 10^{-4}$ (42). In this regard, we note that the magnitude of the shift observed for the g_x component for Sec14p-bound 12-doxyl-PtdCho with respect to that for 16-doxyl-PtdCho is about -5.2×10^{-4} (*i.e.* a value very close to the theoretically predicted shift due to formation of a single hydrogen bond).

The polarity gradient we observe within the Sec14p phospholipid-binding cavity suggests that C_5 of the *sn*-2 acyl chain is located in a relatively polar and protic protein environment,

whereas the environment of the middle of the chain is nonpolar and aprotic. The distal end of the molecule (C_{16}), however, resides in more polar, protic surroundings. These data are most consistent with the bound phospholipid oriented in such a way that the headgroup region is disposed toward solvent, whereas the acyl chains emanate into the hydrophobic interior of the Sec14p phospholipid binding pocket. When coupled with our demonstration of a low accessibility for C_5 to the water-soluble paramagnetic relaxant NiEDDA, we propose the polarity of the Sec14p phospholipid-binding cavity reported by 5-doxyl-PtdCho is not the result of free solvent penetration into this region. Rather, we suggest that our data are indicative of a propensity of the spin label positioned at C_5 to be engaged in hydrogen bonding with neighboring amino acid residues.

DISCUSSION

We describe herein the first spin-labeling EPR experiments to access local dynamics and the electrostatic microenvironment of a PtdCho molecule sequestered within the Sec14p phospholipid-binding pocket. We demonstrate that Sec14p loads effectively with PtdCho species labeled with a doxyl moiety at various positions along the *sn*-2 acyl chain. Once bound, *n*-doxyl-PtdCho species exhibit assignable and informative CW EPR spectral profiles. Analyses of CW EPR spectra from an *n*-doxyl-PtdCho series demonstrate that mobility of the spin label increases in proportion to distance along the *sn*-2 acyl chain from the headgroup/backbone region of Sec14p-bound PtdCho and that this increase in mobility is accompanied by a decrease in anisotropy of motion. These findings indicate that Sec14p invests in tighter interactions with the headgroup/backbone-proximal region of bound phospholipid, whereas interactions with the distal regions of the acyl chains are less robust. The observed decrease in the mobility of the lipid tail can be due to contact with the cavity "floor." It also could indicate interaction of the somewhat polar nitroxide probe with the protein backbone by hydrogen bonding. Although a progressive increase in *sn*-2 acyl chain mobility is observed with distance from the headgroup/backbone region, the overall acyl chain mobility of Sec14p-bound PtdCho remains anisotropic and strongly restricted.

Measurements of the paramagnetic relaxant accessibility to the lipid chain show that positions 5–12 are strongly shielded from hydrophilic solute molecules. The distal acyl chain region of bound phospholipid exhibits limited accessibility to hydrophilic paramagnetic broadening agents (~23% of what would be normally observed for solvent-exposed protein residues). High field EPR experiments also provided evidence for an electrostatic polarity gradient inside the lipid-binding pocket, suggesting a protic electrostatic microenvironment at position C_5 of the *sn*-2 acyl chain with an increasing aproticity as one moves toward the C_{12} of the chain. The more polar, protic environment detected for the distal terminus of the *sn*-2 acyl chain is consistent with higher NiEDDA accessibility or possible interaction with polar protein residues through hydrogen bond formation. Thus, the Sec14p phospholipid-binding pocket provides a hydrophobic matching to accommodate the PtdCho molecule, and the configuration of this electrostatic gradient is most consistent with a headgroup-out orientation of PtdCho within the Sec14p pocket. We propose that this gradient provides the driving thermodynamic force that allows Sec14p to abstract a phospholipid from a membrane bilayer.

Acknowledgments—We thank Eric Ortlund for helpful discussions. We gratefully acknowledge assistance with SR experiments from the National Biomedical EPR Center.

REFERENCES

1. Cleves, A. E., McGee, T. P., and Bankaitis, V. A. (1991) *Trends Cell Biol.* **1,** 30–34
2. Phillips, S. E., Vincent, P., Rizzieri, K., Schaaf, G., Gaucher, E. A., and Bankaitis, V. A. (2006) *Crit. Rev. Biochem. Mol. Biol.* **41,** 1–28
3. Alb, J. G., Jr., Cortese, J. D., Phillips, S. E., Albin, R. L., Nagy, T. R., Hamilton, B. A., and Bankaitis, V. A. (2003) *J. Biol. Chem.* **278,** 33501–33518
4. Yokota, T., Igarashi, K., Uchihara, T., Jishage, K., Tomita, H., Inaba, A., Li, Y., Arita, M., Suzuki, H., Mizusawa, H., and Arai, H. (2001) *Proc. Natl. Acad. Sci. U. S. A.* **98,** 15185–15190
5. Bomar, J. M., Benke, P. J., Slattery, E. L., Puttagunta, R., Taylor, L. P., Seong, E., Nystuen, A., Chen, W., Albin, R. L., Patel, P. D., Kittles, R. A., Sheffield, V. C., and Burmeister, M. (2003) *Nat. Genet.* **35,** 264–269
6. Carmen-Lopez, M., Nicaud, J.-M., Skinner, H. B., Vergnolle, C., Kader, J. C., Bankaitis, V. A., and Gaillardin, C. (1994) *J. Cell Biol.* **124,** 113–127
7. Monteoliva, L., Sanchez, M., Pla, J., Gil, C., and Nombela, C. (1996) *Yeast* **12,** 1097–1105
8. Vincent, P., Chua, M., Nogue, F., Fairbrother, A., Mekheel, H., Xu, Y., Allen, N., Bibikova, T. N., Gilroy, S., and Bankaitis, V. A. (2005) *J. Cell Biol.* **168,** 801–812
9. Sha, B., Phillips, S. E., Bankaitis, V. A., and Luo, M. (1998) *Nature* **391,** 506–510
10. Yoder, M. D., Thomas, L. M., Tremblay, J. M., Oliver, R. L., Yarbrough, L. R., and Helmkamp, G. M., Jr. (2001) *J. Biol. Chem.* **276,** 9246–9252
11. Tilley, S. J., Skippen, A., Murray-Rust, J., Swigart, P. M., Stewart, A., Morgan, C. P., Cockcroft, S., and McDonald, N. Q. (2004) *Structure* **12,** 317–326
12. Altenbach, C., Greenhalgh, D. A., Khorana, H. G., and Hubbell, W. L. (1994) *Proc. Natl. Acad. Sci. U. S. A.* **91,** 1667–1671
13. Smirnova, T. I., Smirnov, A. I., Clarkson, R. B., and Belford, R. L. (1998) *J. Am. Chem. Soc.* **120,** 5060–5072
14. Chen, S. C., Sturtevant, J. M., Conklin, K., and Gaffney, B. J. (1982) *Biochemistry* **21,** 5096–5101
15. Smirnov, A. I., and Belford, R. L. (1995) *J. Magn. Reson. A* **98,** 65–73
16. Smirnova, T. I., Smirnov, A. I., Clarkson, R. B., and Belford, R. L. (1995) *Magn. Reson. Med.* **33,** 801–810
17. Smirnova, T. I., and Smirnov, A. I. (2003) *J. Phys. Chem. B* **107,** 7212–7215
18. Mchaourab, H. S., Lietzow, M. A., Hideg, K., and Hubbell, W. L. (1996) *Biochemistry* **35,** 7692–7704
19. McConnell, H. M., and Hubbell, W. L. (1971) *J. Am. Chem. Soc.* **93,** 314–326
20. Griffith, O. H., and Jost, P. C. (1976) in *Spin Labeling: Theory and Applications* (Berliner, L. J., ed) pp. 454–523, Academic Press, Inc., New York
21. Schorn, K., and Marsh, D. (1997) *Spectrochim. Acta A. Mol. Biomol. Spectrosc.* **53,** 2235–2240
22. Bartucci, R., Belsito, S., and Sportelli, L. (2003) *Chem. Phys. Lipids* **124,** 111–122
23. Isas, J. M., Langen, R., Haigler, H. Y., and Hubbell, W. L. (2002) *Biochemistry* **41,** 1464–1473
24. Altenbach, C., Froncisz, W., Hemker, R., Mchaourab, H., and Hubbell, W. L. (2005) *Biophys. J.* **89,** 2103–2112
25. Hubbell, W. L., Altenbach, C., Hubbell, C. M., and Khorana, H. G. (2003) *Adv. Protein Chem.* **63,** 243–290
26. Hubbell, W. L., Cafiso, D. S., and Altenbach, C. (2000) *Nat. Struct. Biol.* **7,** 735–739
27. Perozo, E. (2002) *Structure* **10,** 1027–1029
28. Perozo, E., Cortes, D. M., and Cuello, L. G. (1999) *Science* **285,** 73–78

29. Han, X., Bushweller, J. H., Cafiso, D. S., and Tamm, L. K. (2001) *Nat. Struct. Biol.* **8,** 715–720
30. Perozo, E., Cortes, D. M., Sompornpisut, P., Kloda, A., and Martinac, B. (2002) *Nature* **418,** 942–948
31. Merianos, H. J., Cadieux, N., Lin, C. H., Kadner, R. J., and Cafiso, D. S. (2000) *Nat. Struct. Biol.* **7,** 205–209
32. Frazier, A. A., Wisner, M. A., Malmberg, J. N., Victor, K. G., Fanucci, G. E., Nalefski, E. A., Falke, J. J., and Cafiso, D. S. (2002) *Biochemistry* **41,** 6282–6292
33. Oh, K. J., Altenbach, C., and Hubbell, W. L. (2000) *Methods Mol. Biol.* **145,** 147–169
34. Robinson, B. H., Haas, D. A., and Mailer, C. (1994) *Science* **263,** 490–493
35. Herschel, W. H. (1917) *U.S. Department of Commerce: Bureau of Standards, Technologic Papers*, Number 100, Government Printing Office, Washington, D.C.
36. Pyka, J., Ilnicki, J., Altenbach, C., Hubbell, W. L., and Froncisz, W. (2005) *Biophys. J.* **89,** 2059–2068
37. Nielsen, R. D., Che, K., Gelb, M. H., and Robinson, B. H. (2005) *J. Am. Chem. Soc.* **127,** 6430–6442
38. Kawamura, T., Matsunami, S., and Yonezawa, T. (1967) *Bull. Chem. Soc. Jap.* **40,** 1111–1115
39. Wegener, C., Savitsky, A., Pfeiffer, M., Möbius, K., and Steinhoff, H.-J. (2001) *Appl. Magn. Reson.* **21,** 441–452
40. Gullá, A. F., and Budil, D. E. (2001) *J. Phys. Chem. B* **105,** 8056–8063
41. Ding, Z., Gullá, A. F., and Budil, D. E. (2001) *J. Chem. Phys.* **115,** 10685–10693
42. Steinhoff, H.-J., Savitsky, A., Wegener, C., Pfeiffer, M., Plato, M., and Möbius, K. (2000) *Biochim. Biophys. Acta* **1457,** 253–262
43. Earle, K. A., Moscicki, J. K., Ge, M., Budil, D., and Freed, J. H. (1994) *Biophys. J.* **66,** 1213–1221
44. Owenius, R., Engström, M., Lindgren, M., and Huber, M. (2001) *J. Phys. Chem. A* **105,** 10967–10977
45. Plato, M., Steinhoff, H.-J., Wegener, C., Torring, J. T., Savitky, A., and Möbius, K. (2002) *Mol. Phys.* **100,** 3711–3721